Ultrasound in Med. & Biol., Vol. 47, No. 11, pp. 3263–3274, 2021

0301-5629/$ - see front matter

https://doi.org/10.1016/j.ultrasmedbio.2021.07.016

● *Original Contribution*

ACOUSTIC DROPLET VAPORIZATION OF PERFLUOROCARBON DROPLETS IN 3D-PRINTABLE GELATIN METHACRYLATE SCAFFOLDS

JENNA OSBORN, MEGAN S. ANDERSON, MORGAN BEDDINGFIELD, LIJIE GRACE ZHANG, and KAUSIK SARKAR
Department of Mechanical and Aerospace Engineering, George Washington University, Washington, DC 20052, USA

(*Received* 23 *February* 2021; *revised* 19 *July* 2021; *in final form* 20 *July* 2021)

Abstract—Scientists face a significant challenge in creating effective biomimetic constructs in tissue engineering with sustained and controlled delivery of growth factors. Recently, the addition of phase-shift droplets inside the scaffolds is being explored for temporal and spatial control of biologic delivery through vaporization using external ultrasound stimulation. Here, we explore acoustic droplet vaporization (ADV) in gelatin methacrylate (GelMA), a popular hydrogel used for tissue engineering applications because of its biocompatibility, tunable mechanical properties and rapid reproducibility. We embedded phase-shift perfluorocarbon droplets within the GelMA resin before crosslinking and characterized ADV and inertial cavitation (IC) thresholds of the embedded droplets. We were successful in vaporizing two different perfluorocarbon—perfluoropentane (PFP) and perfluorohexane (PFH)–cores at 2.25- and 5-MHz frequencies and inside hydrogels with varying mechanical properties. The ADV and IC thresholds for PFP droplets in GelMA scaffolds increased with frequency and in stiffer scaffolds. The PFH droplets exhibited ADV and IC activity only at 5 MHz for the range of excitations below 3MPa investigated here and at threshold values higher than those of PFP droplets. The results provide a proof of concept for the possible use of ADV in hydrogel scaffolds for tissue engineering. (E-mail: sarkar@gwu.edu) © 2021 **World Federation for Ultrasound in Medicine & Biology. All rights reserved.**

Key Words: **Acoustic droplet vaporization, Tissue engineering, Scattering, Perfluorocarbon, Gelatin methacrylate.**

INTRODUCTION

Tissue engineering provides a promising new option for tissue regeneration and creation (Minto et al. 2020). It requires a number of growth factors in the process to successfully mimic the appropriate nature and physiology of the native tissue (Tayalia and Mooney 2009). Growth factors are natural signaling compounds that stimulate or inhibit different cellular processes, such as proliferation, differentiation, adhesion and gene expression (Tayalia and Mooney 2009). In most tissue engineering applications, growth factors are introduced into culture medium, which is not feasible or successful in *in vivo* applications or after implantation (Sahoo et al. 2010). Sustained, controllable and targeted delivery of growth factors remains a challenge. Many researchers have sought to create continuous and controlled delivery systems, but further options are desired (Azizian et al. 2018; Modaresifar et al. 2018). Ultrasound-mediated acoustic vaporization of droplets laden with drugs and growth factors could be an excellent tool for externally controlled spatiotemporal growth factor delivery. Here, we investigate acoustic vaporization of perfluorocarbon droplets embedded in 3D-printed scaffolds of a hydrogel material.

Researchers have explored modifying tissue engineering scaffolds for sustained delivery of growth factors. One method explored has been chemical modification of the scaffold material to include growth factors (Leslie-Barbick et al. 2009; Saik et al. 2011; Zhou et al. 2018). However, while this is successful in many cases, the processes are limited to scaffold materials and therapeutic compounds that can be chemically modified, which limits the applications. Others have explored the embedment of degradable polymeric or liposome-based nanoparticles within the scaffold (MacKinnon et al. 2009; Modaresifar et al. 2018). The encapsulation materials are required to be biodegradable and have a half-life different from that of the surrounding scaffold material (Lee et al. 2011). Some of these techniques can result in a short duration of release, and have a fixed release rate (Lee et al. 2011). To control the time of release or change the rate of release throughout the lifetime of the tissue

Address correspondence to: Kausik Sarkar, George Washington University, 800 22nd Street NW, Suite 3000, Washington DC 20052, USA. E-mail: sarkar@gwu.edu

engineering construct, external stimuli, such as pH changes (Chiu et al. 2009), temperature changes (Ruel-Gariépy et al. 2002), light (Wang et al. 2016) and exposure to electric (Kim et al. 2002) or magnetic (Satarkar and Hilt 2008) fields, have been explored to deliver growth factors on demand (Lee et al. 2011). Recently, ultrasound as an external stimulus has been used because it is safe, non-invasive, inexpensive and widely accessible (Moncion et al. 2016b, 2017, 2018; Aliabouzar et al. 2019a, 2019b, 2020).

Phase-shift droplets have been explored as potential ultrasound contrast agents and drug delivery vehicles (Aliabouzar et al. 2018). These droplets have a volatile perfluorocarbon liquid core, such as perfluoropentane (PFP) or perfluorohexane (PFH). Both of these liquids have boiling points (29°C and 56°C, respectively) lower than that of water and can be vaporized by exposure to low-pressure ultrasound, often dubbed acoustic droplet vaporization (ADV), without vaporizing the surrounding fluid (Kripfgans et al. 2004). When loaded with drugs or growth factors, these particles have substantial promise as a delivery option (Fabiilli et al. 2013). The threshold of peak negative pressure when this vaporization occurs is a highly desired quantity for predicting clinical success and ensuring safety. Moncion et al. (2016a) have found that it is possible to vaporize droplets within fibrinogen hydrogels using external ultrasound stimulation (Moncion et al. 2016b, 2017, 2018). Fibrin, a successful material for tissue engineering, is limited in its use by its stability and low mechanical stiffness (Ahmed et al. 2008). To explore the possibility of extending this work into different tissues, we sought to find other hydrogel alternatives.

Gelatin methacrylate (GelMA) is a popular, inexpensive hydrogel used for tissue engineering applications because of its biocompatibility, tunable mechanical properties and rapid reproducibility (Nichol et al. 2010). With its ability to be crosslinked by ultraviolet (UV) light exposure, GelMA can be 3D printed into a variety of different shapes and geometries customized for patient needs (Zhou et al. 2016). Depending on the concentration and UV crosslinking parameters, the mechanical properties can be altered to customize the hydrogel to different implantation sites, allowing its use for many different regenerative tissue models (Hutson et al. 2011). GelMA has been successfully modified previously for targeted growth factor delivery.

In this proof-of-concept study, perfluorocarbon droplets were embedded within the GelMA resin before 3D printing. The droplets were then vaporized by external acoustic excitations successfully at two different excitation frequencies. We determined the ADV and inertial cavitation (IC) thresholds of embedded droplets with two different perfluorocarbon cores and in GelMA scaffolds with differing stiffness. This method provides a promising option for spatial and temporal control of growth factor delivery in a popular hydrogel with tunable mechanical characteristics for the ability to be used in many different tissue engineering applications.

METHODS

Synthesis of GelMA

We follow a procedure for synthesizing GelMA that has been described previously (Van Den Bulcke et al. 2000; Zhou et al. 2016). Briefly, 10% (w/v) gelatin (Type A, Sigma-Aldrich, St. Louis, MO, USA) was dissolved in heated de-ionized (DI) water while stirring. Next, 4% (v/v) methacrylic anhydride was added dropwise into the solution while stirring. The solution was then stirred for another 2 h while heated. The mixture was dialyzed in DI water for another 6 d to remove excess methacrylic acid. The GelMA was then placed in a lyophilizer for 5−6 d. The resulting powder could be reconstituted with different concentrations of 1% (w/v) photocrosslinker (Irgacure D-2959, Sigma-Aldrich) in DI water for different mechanical properties. Two different concentrations, 10% and 15% (w/v), of GelMA were used in this study.

Synthesis and characterization of perfluorocarbon droplets

We follow the protocol for synthesizing droplets reported in Aliabouzar et al. (2019a). Briefly, 1,2-dipalmitoyl-*sn*-glycero-3-phosphatidylcholine (DPPC), 1,2-dipalmitoyl-*sn*-glycero-3-phosphate, sodium salt (DPPA), and 1,2-dipalmitoyl-*sn*-glycero-3phosphoethanolamine-*N*-[methoxy(polyethylene glycol)-5000] (MPEG5000 DPPE) were set out for 20 min to come to the gel-to-liquid temperature. The solution used to dissolve the lipids was an 8:1:1 volume ratio of phosphate-buffered saline, propylene glycol and glycerol. The propylene glycol was heated to 50°C before dissolving the lipids in an 11:82:7 (DPPA:DPPC:PEG5000) molar ratio. The lipids were dissolved for 20 min before adding the glycerol and phosphate-buffered saline. The lipids were stored for 4°C and used within 1 wk of synthesis.

To make the droplets, 2 mL of the lipid solution was added to 500 μL of PFP, PFH or perfluro-octyl-bromide (PFOB) (Fluromed, Round Rock, TX, USA). The mixture was shaken in a Vial Mixer (Bristol Myers Squibb, North Billerica, MA, USA) at 4800 rpm for 30 s. The vials were stored at 4°C to cool. To eliminate droplets 30 μm in diameter or larger, the droplet solution was diluted to 15 mL in a 15-mL centrifuge tube. The settling times determined from Stokes' Drag Law depended on the core of the droplet (5 min for PFP, 4 min for PFH and 3 min for PFOB).

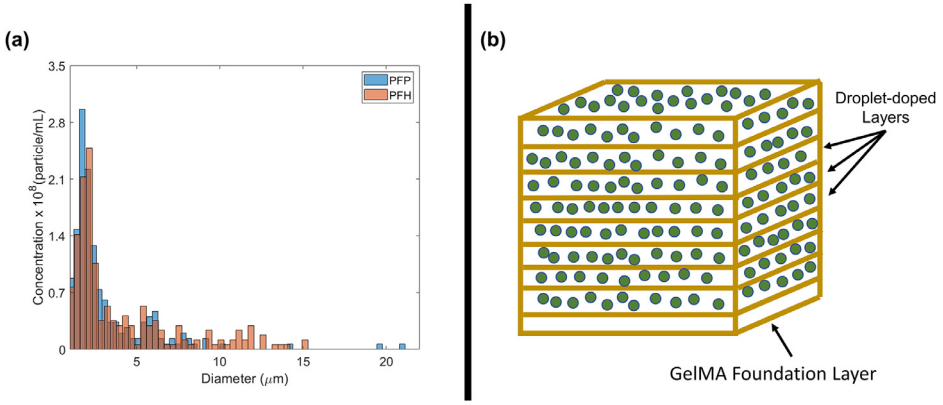

Fig. 1. (a) Size distribution of the perfluoropentane (PFP, *blue*) and perfluorohexane (PFH, *red*) droplets (b) Schematic of the scaffold construction. GelMA = gelatin methacrylate.

The bottom 2 mL of the 15 mL was discarded, and the top 13 mL was used for experiments. The size distribution and concentration of the resultant droplets were measured with a Coulter counter (Multisizer 4, Beckman Coulter, Inc, Indianapolis, IN, USA) in the range 1−30 μm. The size distribution is plotted in Figure 1a, and the average sizes and concentrations of the resultant droplets are tabulated in Table 1.

PRODUCTION OF SCAFFOLDS

To create a scaffold cube, 1 mL of the corresponding concentration of GelMA (without any droplets) was placed in 35-mm petri dish. Then a 3D-printed 2 × 2 × 2-cm cube mold was placed on the petri dish. The GelMA layer on the petri dish was exposed to UV light for 45 s to cross-link it and create a base of the cube. A droplet-doped 1-mL volume of GelMA was pipetted in the mold and cross-linked for the same amount of time, resulting in a 0.25-cm-thick layer (schematic seen in Fig. 1b). This process was repeated for a total of eight layers, resulting in a cube of dimensions 2 × 2 × 2 cm. The cube was removed from the mold and kept in DI water for at least 60 min before being exposed to ultrasound.

MECHANICAL TESTING OF SCAFFOLDS

A compression test was performed on the corresponding scaffolds to determine the compression modulus. A mechanical testing machine (Applied Test Systems, Butler, PA, USA) compressed the scaffolds at the constant rate of 1 mm/min while the load and head displacement were recorded through the experiment. The force and displacement were converted to stress and strain, and a linear curve was fit to the data to extract the compression modulus for strain values from 0.05 to 0.15 (Yoon et al. 2016).

Calibration of spherically focused transducers

All excitation transducers were systematically calibrated with a capsule hydrophone (HGL0200, dynamic range: 1−20 MHz, Onda, Sunnydale, CA, USA) in degassed water. The hydrophone was placed at the focal point of the transducer, and the corresponding received peak-to-peak voltage was recorded. Figure 2 is a schematic of the setup. The voltage levels can be translated to pressure according to the manufacturer's conversion rate. The exciting voltage was kept low for preservation of hydrophone function (0.1−0.4 MPa in peak negative pressure amplitudes after conversion). At low excitation amplitudes, the pressure at the focus p_f can be converted to pressure at the transducer face p_o using the focusing gain G relationship:

$$G = \frac{\pi f_o r_o^2}{c_o F} \tag{1}$$

In this equation, f_o is the central frequency of the transducer, r_o is the transducer radius, c_o is the speed of sound in water and F is the focal length of the transducer. A linear relationship between the exciting voltage of the function generator and the pressure on the transducer

Table 1. Average size and concentration of perfluorocarbon droplets

Perfluorocarbon core	Speed of sound (m/s)	Density at 25°C (kg/m^3)	Bulk boiling point (°C)	Average size (μm)	Concentration (particles/mL)
Perfluoropentane	477	1590	28−30	3.6 ± 1.8	1.4 ± 0.1 × 10^9
Perfluorohexane	548	1648	58−60	3.4 ± 2.8	1.2 ± 0.3 × 10^9

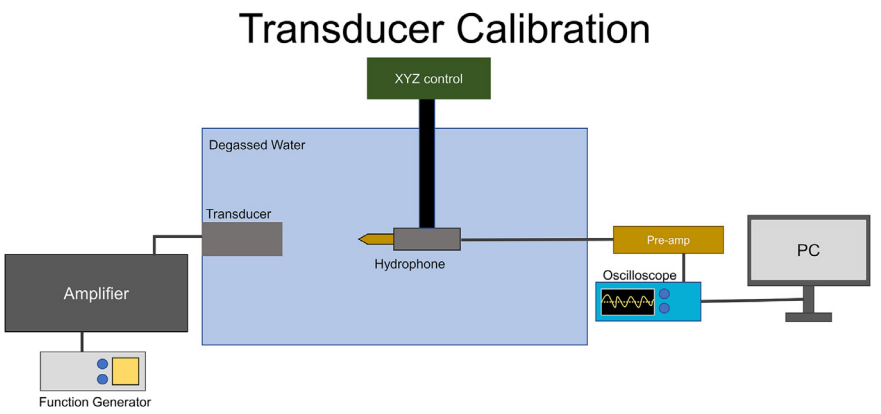

Fig. 2. Experimental setup for calibration of the transmitting transducers.

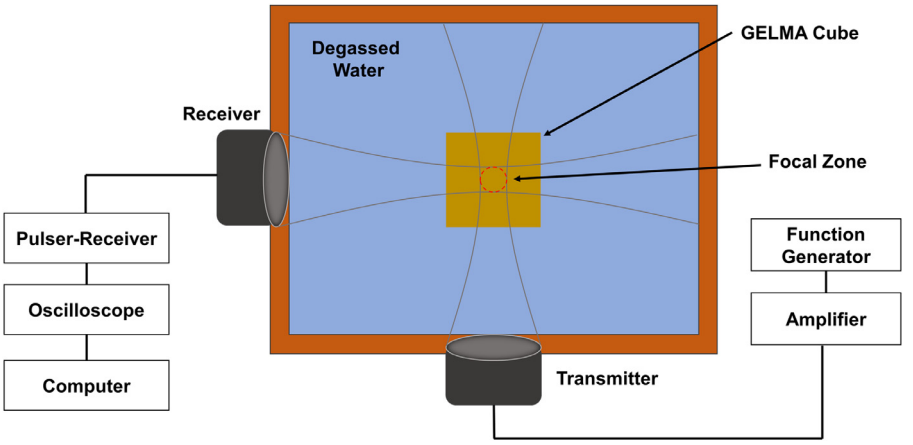

Fig. 3. Experimental setup for ultrasound exposure and gelatin methacrylate (GelMA) cubes.

face was safely assumed for the experimental voltage range and extrapolated to higher amplitudes. To account for the non-linear propagation at higher amplitudes, the Khokhlov–Zabolotskaya–Kusnetsov equation

$$\frac{\partial}{\partial \tau}\left[\frac{\partial p}{\partial z}-\frac{\beta p}{\rho_o c_o^3}\frac{\partial p}{\partial \tau}-\frac{b}{2\rho_o c_o^3}\frac{\partial^2 p}{\partial \tau^2}\right]=\frac{c_o}{2}\Delta_\perp p\pi \qquad (2)$$

was used (Soneson, 2009) to determine the peak positive and negative pressures at the focus as described and verified previously (Canney et al. 2008; Bessonova and Wilkens 2013; Aliabouzar et al. 2019a). In this equation, p is the acoustic pressure, z is the propagation direction, τ is the retarded time (described by $\tau = t - z/c_o$, where t is time), β is the coefficient of non-linearity, b is the dissipation of water and $\Delta_\perp$ is the transverse Laplacian. The boundary conditions used are

$$p(z=0,\ r,\ \tau)=\begin{cases} p_o \sin[\omega_o(\tau + r^2/2c_o F)] & r \le r_o \\ 0 & r > r_o \end{cases} \qquad (3)$$

In this equation, r is the direction perpendicular to the propagation direction.

Ultrasound exposure

The GelMA cube was placed in a custom 3D-printed chamber with confocally aligned transducers. The GelMA cube was placed within the overlapping focal zones as seen in Figure 3. All experiments were performed in de-gassed DI water at 37°C. The cube was exposed to either a 2.25- or 5-MHz excitation 8-cycle pulse with a pulse repetition frequency of 100 Hz for a total of 15 s. The pulse was created with a programmable function generator (DG1022Z, Rigol Technologies, Beijing, China) and amplified with a 55-dB power amplifier (A-150, ENI, Rochester, NY, USA). The amplified signal was used to excite a spherically focused transducer (diameter = 12.7 mm, central frequency = 2.25 MHz, with −6-dB bandwidth:

1.48−2.90 MHz or 5 MHz with −6-dB bandwidth: 3.2−6.5 MHz, focal distance of 30.48 mm) (Olympus NDT, Waltham, MA, USA).

The scattered signal from the scaffolds was received by a cylindrically focused broadband transducer (10 kHz−20 MHz, Sonic Concepts, Bothell, WA, USA) with an active diameter of 17.5 mm and a 50-mm geometric focus. The receiving transducer was connected to a pulser/receiver (5800, Panametrics-NDT, Waltham, MA, USA) in receiving mode with a 20-dB gain (Bandpass filter: 100 kHz−35 MHz). The signals were received by an oscilloscope (Tektronix, MDO3024, Beaverton, OR, USA) to view them during experiments. Fifty signal acquisitions were captured with a customized MATLAB (The MathWorks, Natick, MA, USA) code. The scaffolds were exposed to peak negative pressure amplitudes up to 3.5 MPa. Between excitations, the scaffold was moved so that a new location on it could be excited. For each perfluorocarbon core or scaffold formulation, the vaporization experiment was done three times at different orientations. Embedded PFOB droplets were not seen to vaporize at the frequencies and amplitudes tested and served as a control throughout all experiments (Aliabouzar et al. 2019a).

Determination of ADV and IC threshold

To determine the ADV threshold, a procedure similar to that used by Aliabouzar et al. (2019a) was performed. Briefly, a linear fit to the data was taken at lower peak negative pressure amplitudes. When the data were not represented by the linear fit, another linear fit was taken at the higher amplitudes. The location where the two linear fits intersected was taken to be the ADV threshold. This was performed on the fundamental, subharmonic and second harmonic scattered responses and averaged.

Inertial cavitation is often identified by the presence of broadband signals caused by the violent nature of the bubble collapse (Price et al. 2005). To determine the IC threshold for the droplets embedded within the scaffolds, a process similar to that used for determination of the ADV threshold was followed. Here, unlike in ADV determination, the integrated power frequency spectrum over the low frequency range 400−600 kHz was investigated, as was also done in previous studies (Fabiilli et al. 2009; Aliabouzar et al. 2019a). Two linear fits were performed to the lower integrated powers and the higher integrated powers, respectively, with peak negative pressures. The intersection of the two linear fits was taken as the IC threshold.

Statistical analysis

All results are expressed as the mean and standard deviation (SD), and each scaffold representation was repeated three times. Linear fitting and plotting were performed using MATLAB R2020a.

Table 2. Mechanical properties of scaffolds with different GelMA concentrations and perfluorocarbon cores.

1% (v/v) perfluorocarbon core	GelMA concentration (w/v)	Compression modulus (kPa)
Perfluoropentane	10%	37.3 ± 7.2
	15%	71.0 ± 7.1
Perfluorohexane	10%	37.5 ± 4.2
Perfluro-octyl-bromide	10%	34.7 ± 9.2

GelMA = gelatin methacrylate.

RESULTS

Characterization of scaffolds

The compressional modulus of the scaffolds composed of different GelMA concentrations and corresponding perfluorocarbon cores is outlined in Table 2. The Young's modulus of tissue varies depending on the location within the body. Generally, in soft tissue, it can be anywhere from 0.1 to 700 kPa (Liu et al. 2015). The values found in this study were in that range.

Frequency dependence of ADV thresholds in scaffolds

Ten percent (w/v) GelMA scaffolds were exposed to ultrasound at 2.25 and 5 MHz. The peak negative pressures and resulting scattered fundamental, subharmonic and second harmonic responses at 2.25 MHz are illustrated in Figure 4. The ADV threshold varied only slightly between the different frequency responses–1.03 ± 0.01 MPa from the fundamental (Fig. 4a), 1.23 ± 0.17 MPa from the subharmonic (Fig. 4b) and 1.0 ± 0.22 MPa for the second harmonic (Fig. 4c)–and were averaged. The resulting ADV threshold for the PFP droplets was estimated as 1.09 ± 0.17 MPa when excited at 2.25 MHz. No vaporization for PFH droplets was visualized below a peak negative pressure amplitude of 3 MPa. This pressure amplitude corresponds to a mechanical index of 1.9 for the 2.25-MHz excitation frequency.

For the 5-MHz excitation, the scattered fundamental, subharmonic and second harmonic responses can be seen in Figure 5. For the PFP droplets, the changes in slope in the response occurred at 2.25 ± 0.13 MPa for the fundamental response (Fig. 5a), 2.23 ± 0.17 MPa for the subharmonic response (Fig. 5b) and 2.30 ± 0.13 MPa for the second harmonic (Fig. 5c), resulting in an average ADV threshold of 2.26 ± 0.14 MPa. Note that unlike in Figure 4, in which no ADV were seen at 2.25-MHz stimulation for PFH droplets, here we note a consistent change in slope in the signals for PFH droplets at 2.78 ± 0.05 MPa (fundamental; Fig. 5a), 2.79 ± 0.04 MPa (subharmonic; Fig. 5b) and 2.54 ± 0.20 MPa (second harmonic; Fig. 5c), indicating vaporization. The

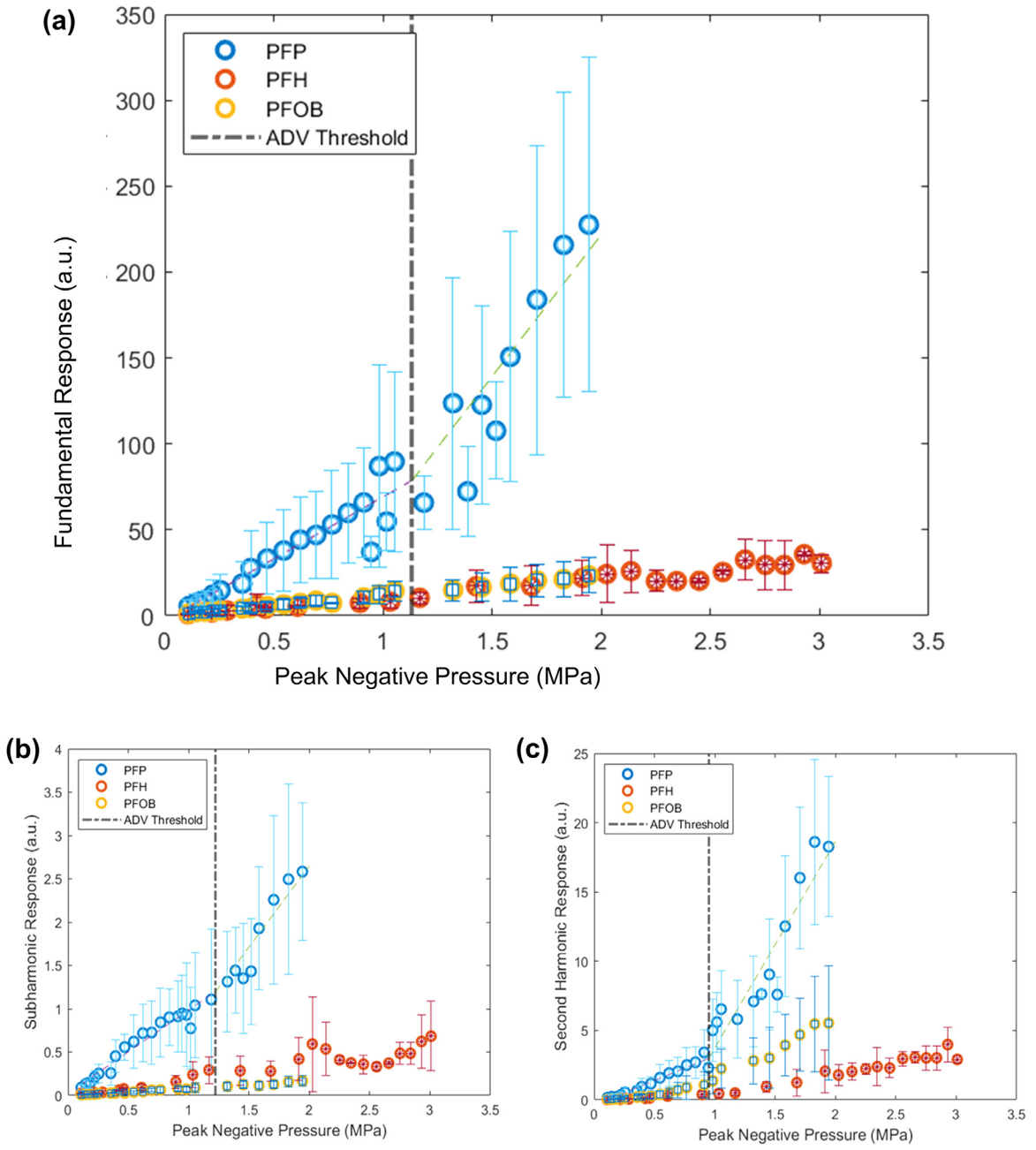

Fig. 4. (a) Fundamental, (b) subharmonic and (c) second harmonic scattered responses to 2.25-MHz ultrasound stimulation in 10% (w/v) gelatin methacrylate scaffolds. The three different cores, PFP (*blue*), PFH (*red*) and PFOB (*yellow*)—are at different peak negative pressure excitation amplitudes. The linear fit used to determine the ADV threshold is shown. ADV = acoustic droplet vaporization; PFP = perfluoropentane; PFH = perfluorohexane; PFOB = perfluoro-octyl-bromide.

average ADV threshold for PFH droplets at 5-MHz stimulation is estimated as 2.71 ± 0.14 MPa. PFH droplets, with a bulk boiling point far above the surrounding temperature of 37°C, likely recondense during the subsequent compression cycle, a phenomenon reported in the literature (Asami and Kawabata 2012; Aliabouzar et al. 2021).

Scaffold mechanical property dependence on ADV threshold

To understand the effects of mechanical properties on the ADV threshold of the droplets, the experiments were repeated on the 15% (w/v) GelMA scaffolds. The scaffolds had 1% (v/v) PFP droplets and were exposed to a 2.25-MHz excitation. The

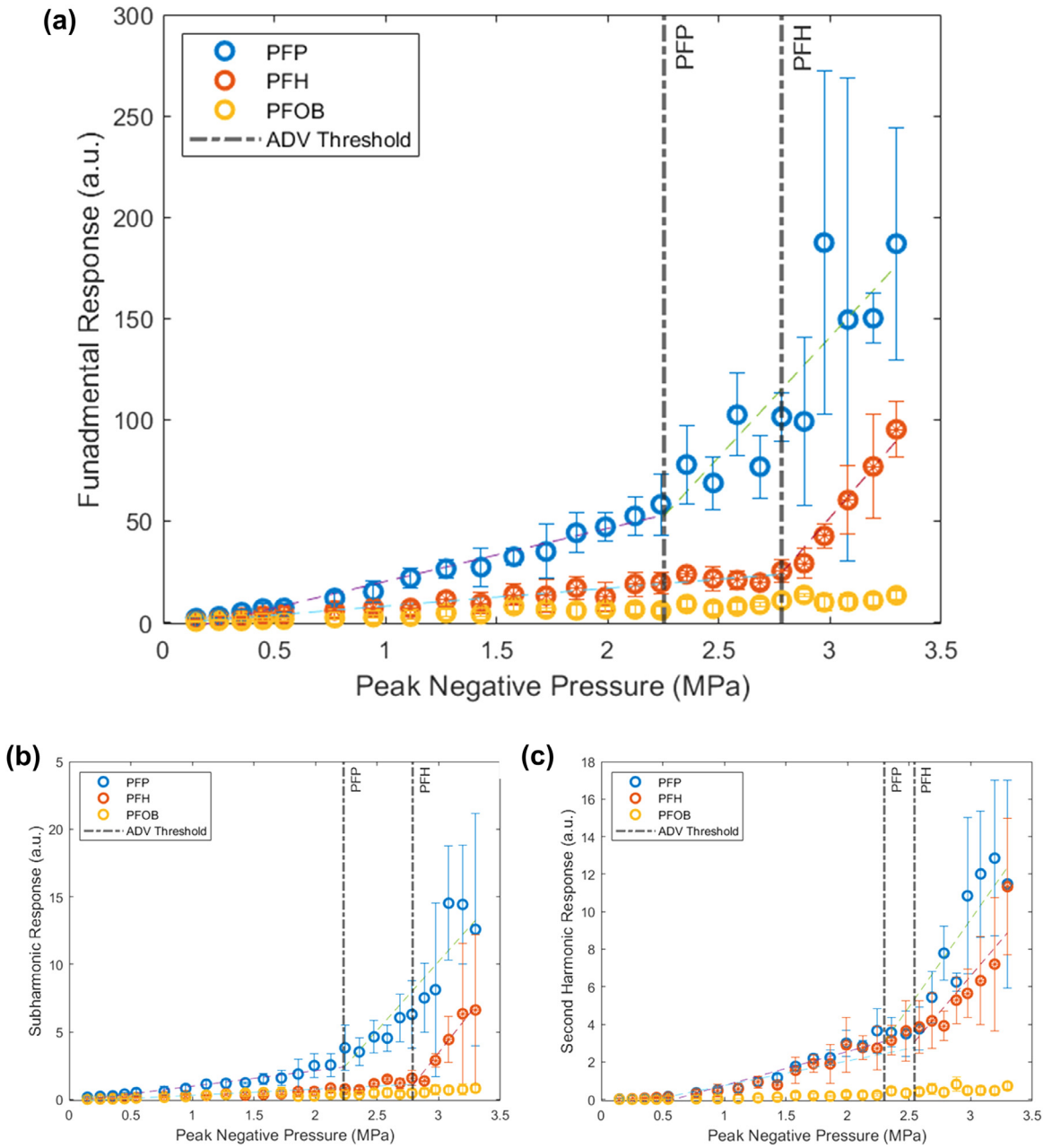

Fig. 5. (a) Fundamental, (b) subharmonic and (c) second harmonic scattered responses to 5- MHz ultrasound stimulation in 10% (w/v) gelatin methacrylate scaffolds. The three different cores—PFP (*blue*), PFH (*red*) and PFOB (*yellow*)—are at different excitation peak negative pressure amplitudes. The linear fit used to determine the ADV threshold is plotted for each perfluorocarbon core. ADV = acoustic droplet vaporization; PFP = perfluoropentane; PFH = perfluorohexane; PFOB = perfluoro-octyl-bromide.

scattered fundamental, subharmonic and second harmonic responses can be seen in Figure 6. As before, each showed a slightly different threshold for change of slope:1.45 ± 0.17 MPa (fundamental; Fig. 6a), 1.32 ± 0.18 MPa (subharmonic; Fig. 6b), 1.30 ± 0.23 MPa (second harmonic; Fig. 6c). The ADV threshold for the 15% (w/v) GelMA cubes with 1% (v/v) PFP droplets was determined to be 1.36 ± 0.18 MPa at 2.25 MPa.

We computed an average ADV threshold at a frequency by averaging over samples taken in three different scaffolds and averaging the ADV thresholds determined from fundamental, subharmonic and second harmonic scattered responses of each scaffold. The

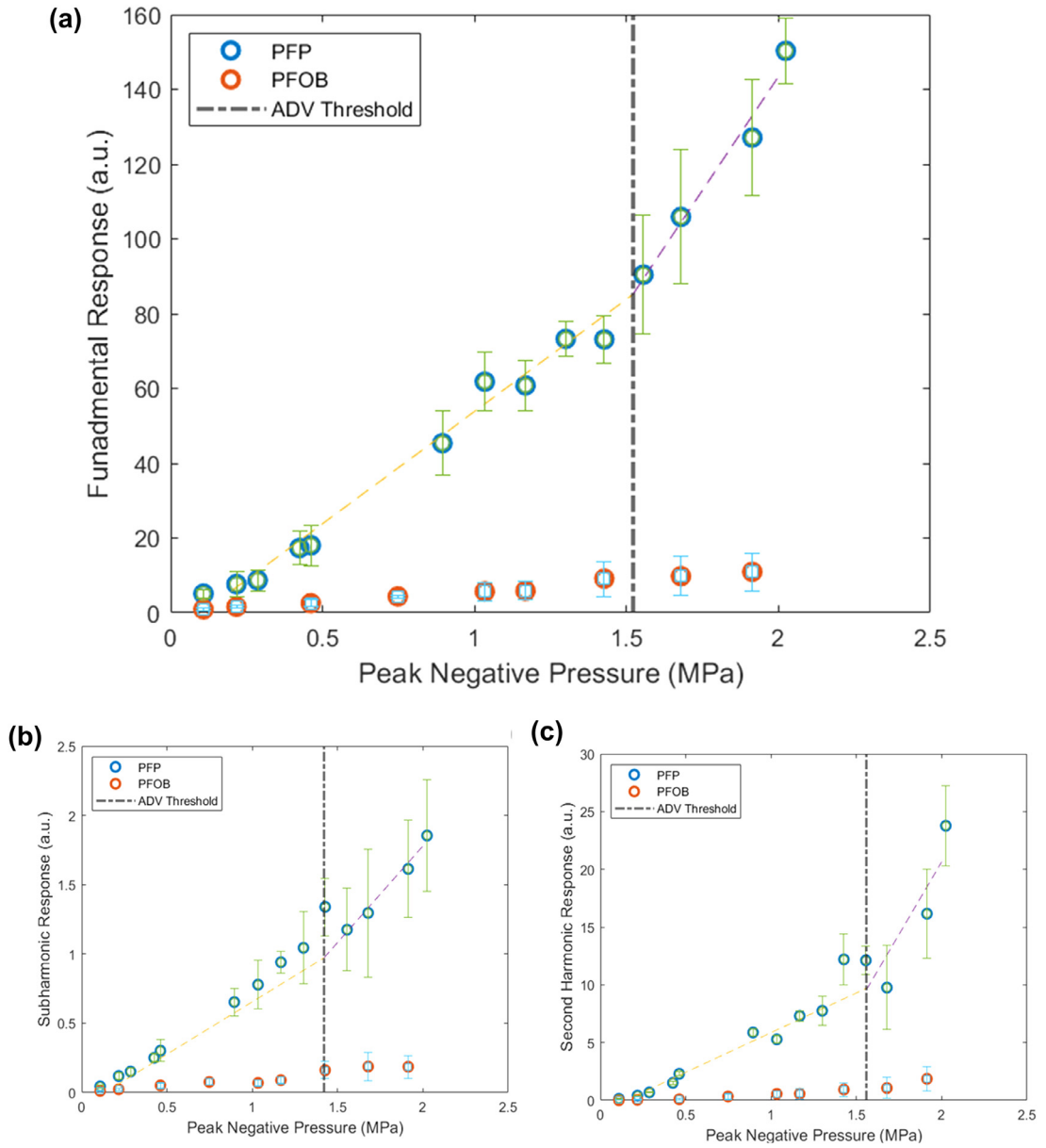

Fig. 6. (a) Fundamental, (b) subharmonic and (c) second harmonic scattered responses to 2.25-MHz ultrasound stimulation in 15% (w/v) gelatin methacrylate scaffolds. The two different cores—PFP (*blue*) and PFOB (*orange*)—at different excitation peak negative pressure amplitudes. The linear fit used to determine the ADV threshold is plotted. ADV = acoustic droplet vaporization; PFP = perfluoropentane; PFOB = perfluoro-octyl-bromide.

ADV threshold increases with frequency for PFP droplets. However, for PFH droplets, although no vaporization was visualized below 3 MPa when excited at 2.25 MHz, a threshold at 2.71 ± 0.14 MPa was observed within this range of excitation (at 5 MHz). Therefore, the ADV threshold for PFH droplets appears to be decreasing with frequency, which can be established only by experiments at higher excitations. The ADV threshold of PFP droplets increased with compressional modulus.

IC threshold in scaffolds

We investigated the integrated power of the scattered pressure from 400 to 600 kHz to determine the IC threshold of the droplets inside the scaffolds. For an excitation frequency of 2.25 MHz, the IC threshold for PFP droplets is 1.72 ± 0.09 MPa (Fig. 7). When excited at 5 MHz, PFP droplets had an IC threshold of 2.81 ± 0.08 MPa and PFH droplets had an IC threshold of 2.87 ± 0.11 MPa (Fig. 8). In 15% (w/v) scaffolds, PFP droplets had an IC threshold of 1.94 ± 0.07 MPa when

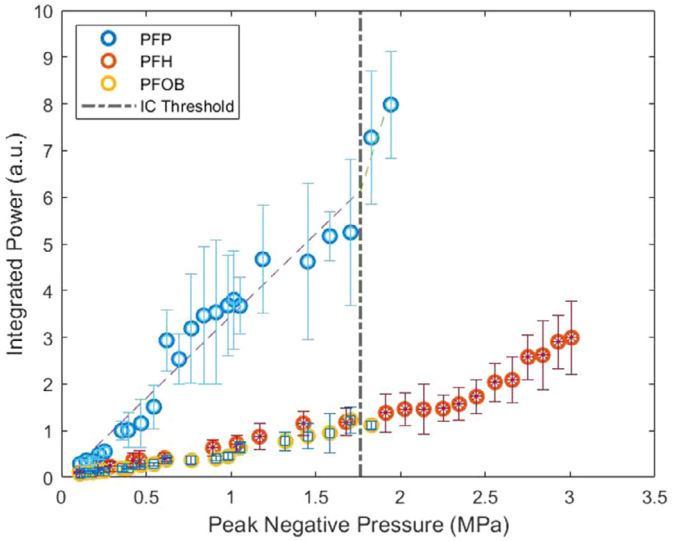

Fig. 7. Integrated power from 10% (w/v) gelatin methacrylate scaffolds excited at 2.25 MHz for the determination of the IC thresholds of three different core droplets: PFP (*blue*), PFH (*red*) and PFOB (*yellow*). IC = inertial cavitation; PFP = perfluoropentane; PFH = perfluorohexane; PFOB = perfluoro-octyl-bromide.

excited at 2.25 MHz (Fig. 9). PFP droplets followed an increasing trend in IC threshold with frequency and compression modulus.

DISCUSSION

The introduction of phase-shift droplets in 3D-printed scaffolds is a promising option for spatiotemporal control of growth factors for tissue engineering applications. Here, we reported ADV within GelMA scaffolds, a commonly used 3D-printable biomaterial. Two different perfluorocarbon cores, PFP and PFH, were successfully vaporized with scaffolds at two different excitation frequencies. To understand the relationship between the ADV and IC thresholds and the mechanical properties of the scaffold, we used two different concentrations of GelMA scaffold, 10% and 15% (w/v).

When compared with the results of droplet vaporization in DI water (Aliabouzar et al. 2019a), the trends

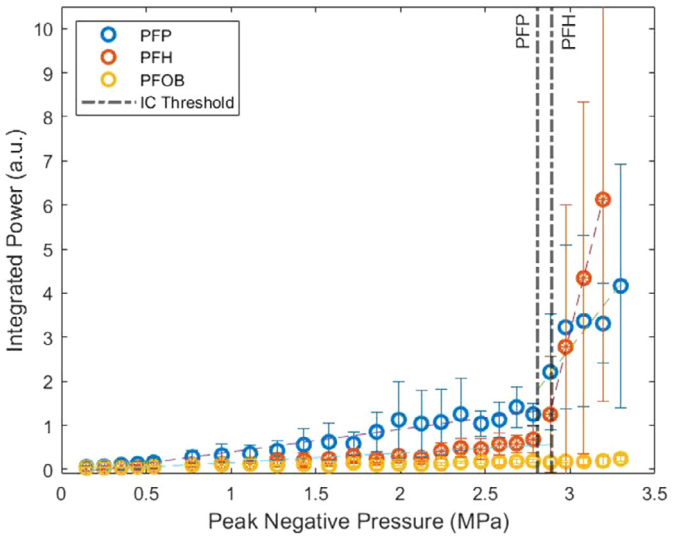

Fig. 8. Integrated power from 10% (w/v) gelatin methacrylate scaffolds excited at 5 MHz for the determination of IC thresholds of three different core droplets: PFP (*blue*), PFH (*red*) and PFOB (*yellow*). IC = inertial cavitation; PFP = perfluoropentane; PFH = perfluorohexane; PFOB = perfluoro-octyl-bromide.

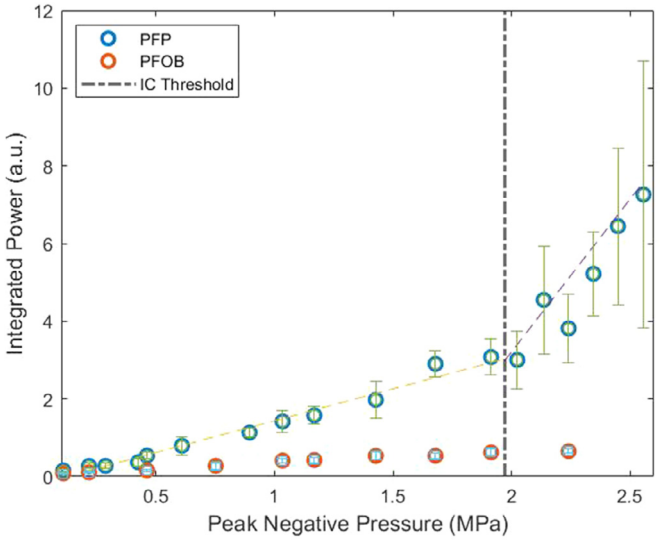

Fig. 9. Integrated power from 15% (w/v) gelatin methacrylate scaffolds excited at 5 MHz for the determination of IC threshold of two different core droplets PFP (*blue*), PFH (*red*) and PFOB (*yellow*). IC = inertial cavitation; PFP = perfluoropentane; PFOB = perfluoro-octyl-bromide.

of ADV and IC thresholds at all frequencies are higher here in scaffolds. PFP droplets in DI water resulted in ADV thresholds of ~0.4 MPa for diameters <3 μm and ~0.5 MPa for diameters >10 μm (Aliabouzar et al. 2019a), a value lower than that (~1 MPa) observed here in GelMA scaffolds. Here, no vaporization for PFH droplets was visualized below peak negative pressure amplitudes of 3 MPa. In DI water, the ADV for PFH droplets occurred above ~2.7 MPa, but only for those that were size selected to be >10 μm. This result is expected because of the higher attenuation of ultrasound as well as higher elasticity of the surrounding scaffold material, which requires a larger amount of acoustic energy for the droplet to vaporize and expand. The ADV threshold with frequency follows a different trend for each of the perfluorocarbon cores. For PFP, the more volatile of the two (bulk boiling point of 29°C), we observed an increasing trend with frequency. This is consistent with our group's previous results using the same droplet composition in DI water (Aliabouzar et al. 2019a). This trend has also been observed by other groups (Kripfgans et al. 2004; Martin et al. 2012; Sheeran et al. 2013). In the previous work performed by Aliabouzar et al. (2019a), the droplets were separated by size into large and small groups. For all sizes of PFP droplets, the ADV threshold was observed to increase with frequency. This trend is attributed to the longer continuous exposure to negative pressure at lower frequencies consistent with classic nucleation theory (Aliabouzar et al. 2019a, Debenedetti 2020).

For PFH droplets, the ADV threshold of the embedded droplets appears to decrease with increasing frequency, in contrast to that for the PFP droplets. On exposure to a 2.25-MHz pulse, vaporization of PFH droplets was not observed below a peak negative pressure amplitude of 3 MPa. In contrast, on exposure to 5-MHz pulses, the PFH droplets vaporized at 2.71 ± 0.14 MPa. This indicates that excitations >3 MPa would be required for vaporization of PFH droplets at 2.25 MHz. Within DI water also, large PFH droplets of the same composition were observed to vaporize at lower peak negative pressure amplitudes with increasing frequency (Aliabouzar et al. 2019a). This decreasing trend with frequency is likely owing to the superharmonic focusing present within larger droplets. The effect combines the non-linear propagation of an acoustic wave at higher pressure amplitudes, and in the presence of a droplet, the wave will focus inside the droplet to much higher amplitudes of pressure (Shpak et al. 2014). This has been reported to be prominent for droplets with a radius >4 μm (Shpak et al. 2014). The larger droplets seem to be driving the vaporization behavior of PFH droplets visualized in this study. This result is different from the work on fibrin scaffolds with PFH double emulsions, where an increasing trend in ADV threshold with frequency is observed (Aliabouzar et al. 2019b). This difference may be attributable to the difference in droplet

shell characteristics or the double-emission nature of droplets used in those studies (Moncion et al. 2016a).

GelMA scaffold material properties can be varied with different concentrations, UV crosslinking parameters and concentrations of photo-initiator (Rizwan et al. 2020). To illustrate the applications of the ADV in GelMA scaffolds to a wide variety of tissue engineering applications, two different concentrations were tested to determine the ADV and IC thresholds. GelMA concentrations of 10% (w/v) and 15% (w/v) are commonly used concentrations in tissue scaffold production (Yoon et al. 2016; Zhou et al. 2017, 2018; Cui et al. 2019). It is critical for the scaffold material to closely mimic the native tissue environment. The material properties (compression modulus 30−45 kPa) of the 10% (w/v) GelMA scaffolds are similar to those of native breast, uterine and muscle tissue (Wells and Liang 2011). The 15% (w/v) GelMA scaffolds have material properties (compression modulus: 65−75 kPa) similar to those of cervical, prostate and muscle tissue (Wells and Liang 2011). The ADV threshold at 2.25 MHz increased with compression modulus of the scaffolds for the PFP droplets. This result is expected as the 15% (w/v) scaffolds are stiffer and require more energy to vaporize the embedded droplets.

The IC thresholds followed trends similar to those of the ADV thresholds in the scaffolds tested here. The IC thresholds were always higher than the ADV thresholds for all cases. This relationship between ADV and IC thresholds is consistent with results observed previously in DI water of the same droplet composition by our group (Aliabouzar et al. 2019a). The trend in IC threshold for PFP droplets increased with frequency and with compression modulus of the scaffolds.

CONCLUSIONS

The goal of this study was to explore the possibility of using acoustically responsive droplets embedded in GelMA for applications for delivery of growth factors in tissue engineering scaffolds. Sustained, spatiotemporally controlled delivery of growth factors remains a challenge for tissue engineering. Within this study, we successfully vaporized droplets with PFP and PFH cores with two different frequencies of ultrasound. The ADV threshold for droplets with PFP cores were observed to increase with frequency when embedded with droplets. Droplets with PFH cores were observed to decrease with frequency in scaffolds. To understand the relationship between ADV threshold and mechanical properties, two different GelMA concentrations were tested. The ADV threshold was observed to increase with increasing compression modulus. The successful droplet vaporization within these two commonly used GelMA formulations provides evidence that this method could be used for a variety of applications. The use of ADV for delivery of growth factors provides a promising option for tissue engineering.

DECLARATION OF COMPETING INTEREST

The authors declare they have no conflicts of interest.

Acknowledgments—The authors thank the Division of Applied Mechanics, Office of Science and Engineering Laboratories, U.S. Food and Drug Administration, for allowing them to use the Coulter counter. In addition, the authors thank the family of the late Michael Myers for funding support. K.S. acknowledges partial support from National Science Foundation Awards 2037849 and 1603639.

REFERENCES

Ahmed TA, Dare EV, Hincke M. Fibrin: A versatile scaffold for tissue engineering applications. Tissue Eng Part B Rev 2008;14:199–215.

Aliabouzar M, Kumar KN, Sarkar K. Acoustic vaporization threshold of lipid-coated perfluoropentane droplets. J Acoust Soc Am 2018;143:2001–2012.

Aliabouzar M, Kumar KN, Sarkar K. Effects of droplet size and perfluorocarbon boiling point on the frequency dependence of acoustic vaporization threshold. J Acoust Soc Am 2019a;145:1105–1116.

Aliabouzar M, Lu X, Kripfgans OD, Fowlkes JB, Fabiilli ML. Acoustic droplet vaporization in acoustically responsive scaffolds: Effects of frequency of excitation, volume fraction and threshold determination method. Ultrasound Med Biol 2019b;45:3246–3260.

Aliabouzar M, Davidson CD, Wang WY, Kripfgans OD, Franceschi RT, Putnam AJ, Fowlkes JB, Baker BM, Fabiilli ML. Spatiotemporal control of micromechanics and microstructure in acoustically-responsive scaffolds using acoustic droplet vaporization. Soft Matter 2020;16:6501–6513.

Aliabouzar M, Kripfgans OD, Wang WY, Baker BM, Brian Fowlkes J, Fabiilli ML. Stable and transient bubble formation in acoustically-responsive scaffolds by acoustic droplet vaporization: Theory and application in sequential release. Ultrason Sonochem 2021;72 105430.

Asami R, Kawabata K. Repeatable vaporization of optically vaporizable perfluorocarbon droplets for photoacoustic contrast enhanced imaging. Proc Int IEEE Ultrason Symp 2012;100–1203.

Azizian S, Hadjizadeh A, Niknejad H. Chitosan-gelatin porous scaffold incorporated with chitosan nanoparticles for growth factor delivery in tissue engineering. Carbohydr Polym 2018;202:315–322.

Bessonova OV, Wilkens V. Membrane hydrophone measurement and numerical simulation of HIFU fields up to developed shock regimes. IEEE Trans Ultrason Ferroelectr Freq Control 2013;60:290–300.

Canney MS, Bailey MR, Crum LA, Khokhlova VA, Sapozhnikov OA. Acoustic characterization of high intensity focused ultrasound fields: A combined measurement and modeling approach. J Acoust Soc Am 2008;124:2406–2420.

Chiu YL, Chen SC, Su CJ, Hsiao CW, Chen YM, Chen HL, Sung HW. pH-Triggered injectable hydrogels prepared from aqueous *N*-palmitoyl chitosan: In vitro characteristics and in vivo biocompatibility. Biomaterials 2009;30:4877–4888.

Cui H, Zhu W, Huang Y, Liu C, Yu ZX, Nowicki M, Miao S, Cheng Y, Zhou X, Lee SJ, Zhou Y, Wang S, Mohiuddin M, Horvath K, Zhang LG. In vitro and in vivo evaluation of 3D bioprinted small-diameter vasculature with smooth muscle and endothelium. Biofabrication 2019;12 015004-04.

Debenedetti PG. Metastable liquids: Concepts and principles. Princeton, NJ: Princeton University Press; 2020.

Fabiilli ML, Haworth KJ, Fakhri NH, Kripfgans OD, Carson PL, Fowlkes JB. The role of inertial cavitation in acoustic droplet vaporization. IEEE Trans Ultrason Ferroelectr Freq Control 2009;56:1006–1017.

Fabiilli ML, Wilson CG, Padilla F, Martín-Saavedra FM, Fowlkes JB, Franceschi RT. Acoustic droplet-hydrogel composites for spatial and temporal control of growth factor delivery and scaffold stiffness. Acta Biomater 2013;9:7399–7409.

Hutson CB, Nichol JW, Aubin H, Bae H, Yamanlar S, Al-Haque S, Koshy ST, Khademhosseini A. Synthesis and characterization of tunable poly(ethylene glycol): Gelatin methacrylate composite hydrogels. Tissue Eng Part A 2011;17:1713–1723.

Kim SJ, Park SJ, Kim IY, Shin MS, Kim SI. Electric stimuli responses to poly(vinyl alcohol)/chitosan interpenetrating polymer network hydrogel in NaCl solutions. J Appl Polym Sci 2002;86:2285–2289.

Kripfgans OD, Fabiilli ML, Carson PL, Fowlkes JB. On the acoustic vaporization of micrometer-sized droplets. J Acoust Soc Am 2004;116:272–281.

Lee K, Silva EA, Mooney DJ. Growth factor delivery-based tissue engineering: General approaches and a review of recent developments. J R Soc Interface 2011;8:153–170.

Leslie-Barbick JE, Moon JJ, West JL. Covalently-immobilized vascular endothelial growth factor promotes endothelial cell tubulogenesis in poly(ethylene glycol) diacrylate hydrogels. J Biomater Sc Polym Ed 2009;20:1763–1779.

Liu J, Zheng H, Poh PSP, Machens HG, Schilling AF. Hydrogels for engineering of perfusable vascular networks. Int J Mol Sci 2015;16:15997–16016.

MacKinnon N, Guérin G, Liu B, Gradinaru CC, Macdonald PM. Liposome−hydrogel bead complexes prepared via biotin−avidin conjugation. Langmuir 2009;25:9413–9423.

Martin AL, Seo M, Williams R, Belayneh G, Foster FS, Matsuura N. Intracellular growth of nanoscale perfluorocarbon droplets for enhanced ultrasound-induced phase-change conversion. Ultrasound Med Biol 2012;38:1799–1810.

Minto J, Zhou X, Osborn J, Zhang LG, Sarkar K, Rao RD. Three-dimensional printing: A catalyst for a changing orthopaedic landscape. JBJS Rev 2020;8:e0076.

Modaresifar K, Hadjizadeh A, Niknejad H. Design and fabrication of GelMA/chitosan nanoparticles composite hydrogel for angiogenic growth factor delivery. Artif Cells Nanomed Biotechnol 2018;46:1799–1808.

Moncion A, Arlotta KJ, Kripfgans OD, Fowlkes JB, Carson PL, Putnam AJ, Franceschi RT, Fabiilli ML. Design and characterization of fibrin-based acoustically responsive scaffolds for tissue engineering applications. Ultrasound Med Biol 2016a;42:257–271.

Moncion A, Arlotta KJ, O'Neill EG, Lin M, Mohr LA, Franceschi RT, Kripfgans OD, Putnam AJ, Fabiilli ML. In vitro and in vivo assessment of controlled release and degradation of acoustically responsive scaffolds. Acta Biomater 2016b;46:221–233.

Moncion A, Lin M, O'Neill EG, Franceschi RT, Kripfgans OD, Putnam AJ, Fabiilli ML. Controlled release of basic fibroblast growth factor for angiogenesis using acoustically-responsive scaffolds. Biomaterials 2017;140:26–36.

Moncion A, Lin M, Kripfgans OD, Franceschi RT, Putnam AJ, Fabiilli ML. Sequential payload release from acoustically-responsive scaffolds using focused ultrasound. Ultrasound Med Biol 2018;44:2323–2335.

Nichol JW, Koshy ST, Bae H, Hwang CM, Yamanlar S, Khademhosseini A. Cell-laden microengineered gelatin methacrylate hydrogels. Biomaterials 2010;31:5536–5544.

Price GJ, Ashokkumar M, Hodnett M, Zequiri B, Grieser F. Acoustic emission from cavitating solutions: Implications for the mechanisms of sonochemical reactions. J Phys Chem B 2005;109:17799–17801.

Rizwan M, Chan SW, Comeau PA, Willett TL, Yim EKF. Effect of sterilization treatment on mechanical properties, biodegradation, bioactivity and printability of GelMA hydrogels. Biomed Mater 2020;15 065017.

Ruel-Gariépy E, Leclair G, Hildgen P, Gupta A, Leroux JC. Thermosensitive chitosan-based hydrogel containing liposomes for the delivery of hydrophilic molecules. J Control Release 2002;82:373–383.

Sahoo S, Ang LT, Goh JC, Toh SL. Growth factor delivery through electrospun nanofibers in scaffolds for tissue engineering applications. J Biomed Mater Res A 2010;93:1539–1550.

Saik JE, Gould DJ, Watkins EM, Dickinson ME, West JL. Covalently immobilized platelet-derived growth factor-BB promotes angiogenesis in biomimetic poly(ethylene glycol) hydrogels. Acta Biomater 2011;7:133–143.

Satarkar NS, Hilt JZ. Magnetic hydrogel nanocomposites for remote controlled pulsatile drug release. J Control Release 2008;130:246–251.

Sheeran PS, Matsunaga TO, Dayton PA. Phase-transition thresholds and vaporization phenomena for ultrasound phase-change nanoemulsions assessed via high-speed optical microscopy. Phys Med Biol 2013;58:4513–4534.

Shpak O, Verweij M, Vos HJ, de Jong N, Lohse D, Versluis M. Acoustic droplet vaporization is initiated by superharmonic focusing. Proc Natl Acad Sci USA 2014;111:1697–1702.

Soneson JE. A user-friendly software package for HIFU simulation. AIP Conf Proc 2009;1113:165–169.

Tayalia P, Mooney DJ. Controlled growth factor delivery for tissue engineering. Adv Mater 2009;21:3269–3285.

Van Den Bulcke AI, Bogdanov B, De Rooze N, Schacht EH, Cornelissen M, Berghmans H. Structural and rheological properties of methacrylamide modified gelatin hydrogels. Biomacromolecules 2000;1:31–38.

Wang X, Wang C, Zhang Q, Cheng Y. Near infrared light-responsive and injectable supramolecular hydrogels for on-demand drug delivery. Chem Commun 2016;52:978–981.

Wells PNT, Liang HD. Medical ultrasound: Imaging of soft tissue strain and elasticity. J R Soc Interface 2011;8:1521–1549.

Yoon HJ, Shin SR, Cha JM, Lee SH, Kim JH, Do JT, Song H, Bae H. Cold water fish gelatin methacryloyl hydrogel for tissue engineering application. PLoS One 2016;11 e0163902.

Zhou X, Zhu W, Nowicki M, Miao S, Cui H, Holmes B, Glazer RI, Zhang LG. 3D bioprinting a cell-laden bone matrix for breast cancer metastasis study. ACS Appl Mater Interfaces 2016;8:30017–30026.

Zhou X, Nowicki M, Cui H, Zhu W, Fang X, Miao S, Lee SJ, Keidar M, Zhang LG. 3D bioprinted graphene oxide-incorporated matrix for promoting chondrogenic differentiation of human bone marrow mesenchymal stem cells. Carbon 2017;116:615–624.

Zhou X, Cui H, Nowicki M, Miao S, Lee SJ, Masood F, Harris BT, Zhang LG. Three-dimensional-bioprinted dopamine-based matrix for promoting neural regeneration. ACS Appl Mater Interfaces 2018;10:8993–9001.